Harvesting electrical energy from water drops falling on a vibrating cantilever

L.E. Helseth

Department of Physics and Technology, Allegaten 55, 5020 Bergen, University of Bergen, Norway

ABSTRACT: In this work a novel thin-film device combining piezoelectric and contact electrification energy harvesting is created with the aim of investigating how it responds to water droplet impact during vibrations. The two energy harvesting principles utilize the same ground electrode, but the electrical signal outputs are independent and show entirely different electrical signal characteristics in presence of external forcing. While piezoelectricity gives rise to a nearly quadratic increase in harvested energy as a function of vibration velocity, the energy due to contact electrification reaches saturation for larger water drop velocities. On the other hand, when the water stream transitions from discrete droplets to a continuous stream the energy gathered from the piezoelectric mechanism exhibits saturation, whereas the energy due to contact electrification decreases. The proposed device may have applications as a self-powered environmental sensor that allow one to distinguish between forced oscillations and water droplet impacts.

KEYWORDS: Piezoelectric, contact electrification, renewable energy

1. Introduction

Small scale energy harvesting from multiple sources of mechanical energy in the environment is gradually playing a more important role in a society aiming for optimal use of localized renewable energy. To date, several different physical principles for gathering electrical energy have been considered. Piezoelectric materials have been under investigation for more than two decades due to their ability of transforming the mechanical energy associated with impact [1] or vibrations [2,3] into electrical energy that drive self-powered sensors [4,5] stored in supercapacitors or batteries [6]. Flow induced vibrations [7-10] as well as impact from water droplets [11] are both sources of mechanical energy that can be transformed into electrical energy. Both single [12-15] and multiple harvesting units [16,17] have been considered. The performance is influenced by a range of different properties, such as cantilever length [18], wetting properties [19] and the fluid layer thickness [20].

While piezoelectric energy harvesting systems have been studied in detail and found to have considerable potential, their impact could be increased further in a combination with other types of energy harvesting. It has long been known that electrical charge transfer occurs when liquids come in contact with different surfaces [21-25]. The charge transfer efficiency depends on a range of parameters such as surface precharge [26], ion type and concentration [23,27-30], surface roughness [31], flow rate [32,33] and droplet impact parameters [32,34,35]. Contact electrification has been utilized in sensors [36-39] or for energy harvesting [40-47]. In particular, the liquid contact charge transfer allows for design of self-powered sensors for level-monitoring [48], for applications in microfluidics [49,50], distress signal emission [51] and in optical communications [52,53]. The active elements can, in addition to water droplets, also be air bubbles [54] or fluid elements [55,56], and self-powered sensors for monitoring parameters such as ion concentration [57], liquid leakages [58], turbidity [59] and pH [60] have been constructed. In designing a self-powered sensor based on contact electrification, the surface composition [61-66], surface structure [67-72] and electrode arrangement [73-76] are of importance. Recent studies

have demonstrated that electrodes mounted on the front surface facing the water droplet may provide higher power output than back-electrodes that never come in contact with water [77-82].

Contact electrification has recently also been suggested in combination with piezoelectricity for devices harvesting electrical energy from water droplets [83]. When combining energy harvesting systems in a single system it is important to create a design that utilizes the strengths of the individual parts [33,84,85]. Further development of combined water drop energy harvesting devices requires a profound understanding of how the piezoelectric and contact electric power contribute to the total harvested electrical power under different situations. For example, piezoelectricity may be used to harvest energy from forced oscillations of the entire device, whereas contact electrification relies on impact and movement of a dielectric like water across an interface. Therefore, the two energy harvesting modes react differently to forced oscillations and impact forces. However, no such studies reporting the combination of forced oscillations and impact forces on combined water droplet energy devices have been reported. In the current study, a device combining piezoelectricity and contact electrification is studied with the aim of investigating its behavior in presence of both impacting water droplets and forced fluctuations. By doing such a study, better insight is gained into the strengths of the two principles, for example if one in the future aim to employ such energy harvesting structures in environments were both wind and rain is present.

2. Experimental setup

The performance of piezoelectric energy harvesters depends on their geometry and position of proof mass [86,87]. For harvesting using water drops, it is most convenient to utilize a flexible and rectangular thin film such as that used in in ref. [15] is preferred. The device presented in this work was made by modifying a commercially available piezoelectric sensor (DT1-028K/L from Measurement Specialities) consisting of a 28 μm thick polyvinylidene fluoride (PVDF) film with silver ink screen printed electrodes. The manufacturer reports piezo strain constants of $d_{31}=23\cdot10^{-12}$ C/N and $d_{33}=-33\cdot10^{-12}$ C/N. The specific

piezoelectric device selected here was chosen since it is a thin, flexible film that bends upon impact and allows water droplets to easily roll off. Moreover, it is thin enough to allow efficient back-electrode coupling and corresponding charge transfer when combined with a contact electric film mounted on top of it. To this end, a 50 μm thick fluorinated ethylene propylene (FEP) film (DuPont) of approximately the same lateral dimensions as the piezoelectric sensor was glued with a very thin layer of polydimethylsiloxane (PDMS) onto the PVDF film. This resulted in an upper surface made of FEP known to provide relatively charge transfer upon contact with water [31,32].

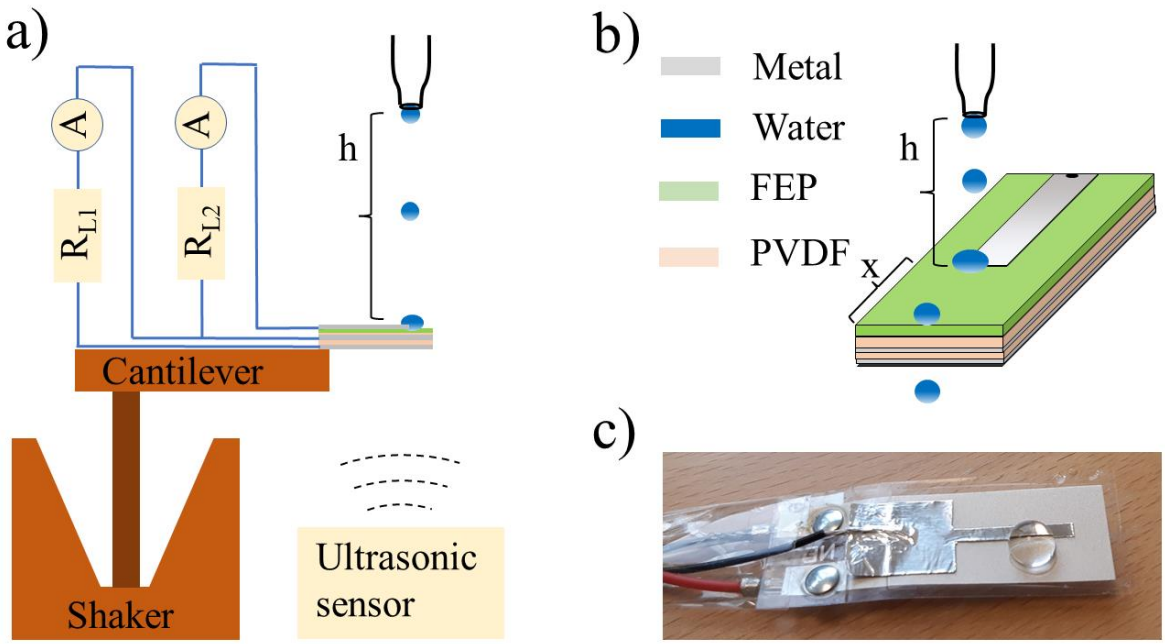

Figure 1. The figure shows a schematic drawing of a water droplet impinging on the combined device consisting of triboelectric and piezoelectric generators (a). Here R_{L1} and R_{L2} are the load resistors connected to the piezoelectric and triboelectric devices, respectively. The encircled latter A refers to the amperemeters used. A more detailed schematic drawing of the energy harvesting device is shown in b), while an actual picture of the device is shown in c).

The electrodes and the underside were also covered by a thin layer of PDMS to ensure that the entire device was waterproof. Next, a 0.1 mm thin film of aluminum was glued on the top of the FEP film as shown in fig. 1. The aluminum film was 2 mm in width and its far edge located 5 mm from the edge of the FEP. A thin layer of PDMS was dropped on top of the exposed wire connected to aluminum film in order to prevent it from getting wet during experiments.

One end of the device shown in figure 1 was glued to an electromagnetic shaker (Smart Materials GmbH) which was vibrated at frequencies up to 8 Hz with controllable amplitude, see also ref. [42]. The other end of the device was free, giving a 16 mm wide and approximately 40 mm long thin-film 'beam' that could be vibrated by the electromagnetic shaker. This beam, being a thin film composite moved in a flapping manner. The velocity of the vibrating devices was measured using an ultrasonic sensor (Vernier) to an accuracy of 0.05 m/s. Water was taken from a Milipore system providing ultrapure water (18.2 MΩcm, Millipore), which upon use had a resistivity of about 1 MΩcm due to contact with CO_2 in the air as well as the walls of the plastic container. Water droplets were released from a variable height at a variable rate, using a dropper connected to a water reservoir, see also Refs. [31-33]. A Keithley 6514 instrument was used to measure the electrical voltage and current. When the currents due to piezoelectricity and contact electrification were measured simultaneously, this was done using the Keithley 6514 together with a Keithley 6485 picoamperemeter as shown in figure 1 a).

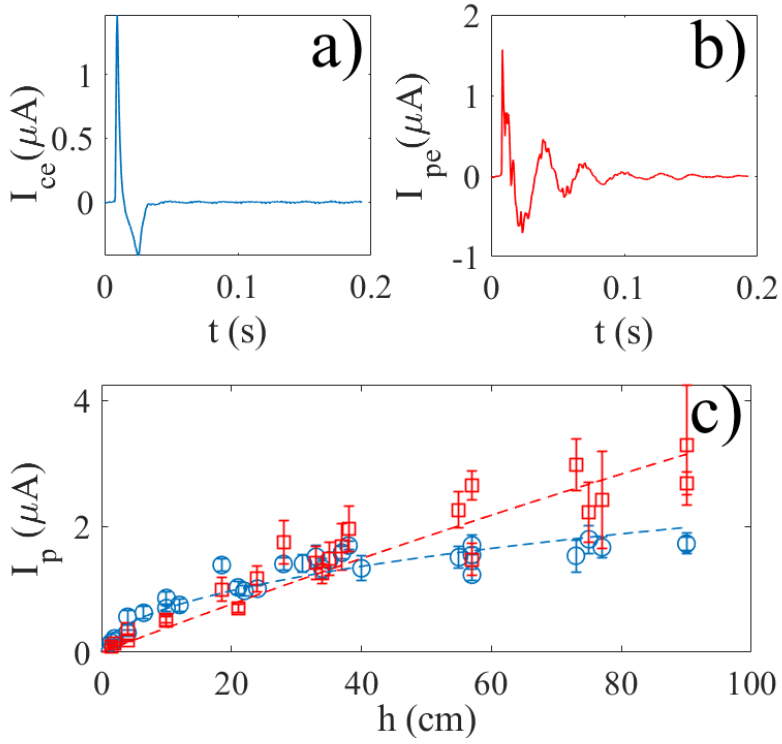

Figure 2. The short circuit current due to contact charge transfer (a) and piezoelectricity (b) upon impact of a single 50 µL water drop impinging from a height h=37 cm. In c) the peak current is shown as a function of falling height of the water drop for the contact charge transfer (circles) and the piezoelectricity (squares), where the blue dashed line is a fit of equation (6) to the experimental data and the red dashed line is a fit of equation (10) to the experimental data.

Figure 2 a) and b) show the short circuit current due to piezoelectricity and contact electrification in absence of cantilever oscillations for a single 50 µL water drop impinging from a height h=37 cm. The signal due to contact charge transfer exhibits a sharp increase to a peak current $I_p \approx 1.5$ µA, followed by a return current, much in the same manner as reported and explained in Ref. [59]. The duration of the pulse is about 20 ms. The piezoelectric current was recorded simultaneously and exhibited a sharp increase to a peak current $I_p \approx 1.5$ µA before decaying oscillations set in for about 100 ms. These oscillations are well-known for other piezoelectric devices mounted on cantilevers as explained in Refs. [11-15]. Here, the

oscillations appear slightly irregular compared to the literature since a flexible film, not a stiff beam, act as the cantilever.

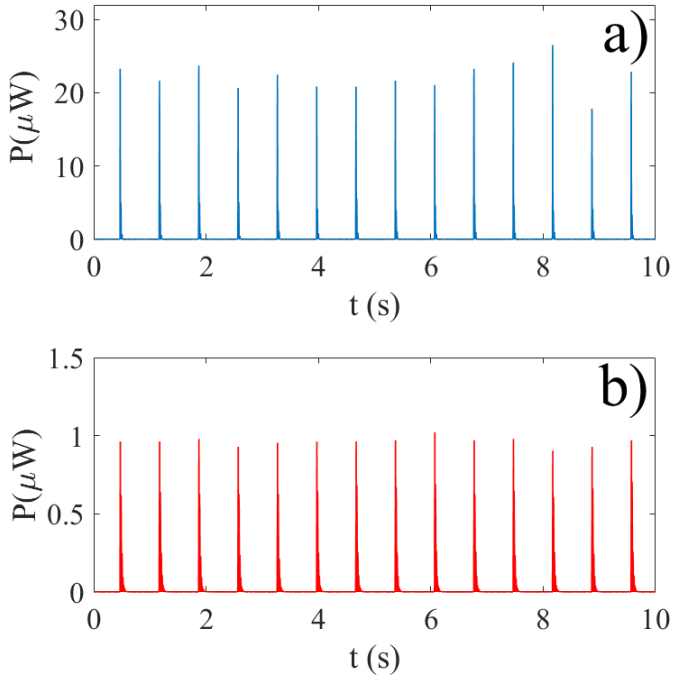

Figure 3. The instantaneous electrical power as a function of time due to contact electrification (a) and piezoelectricity (b) with load resistance of 50 MΩ and 2 MΩ, respectively. Both signals have been recorded simultaneously for 50 μL water droplets impinging from a height of h=57 cm.

A load resistance R_L was inserted in the electrical circuits in figure 1 a). Upon measuring the current through a resistor for a given load resistance, the instantaneous power can be computed as $P(t)=R_L I^2(t)$. Figure 3 a) shows the instantaneous electrical power as a function of time due to contact electrification for a R_L=50 MΩ load when water droplets of volume 50 μL were released from h=57 cm. It is seen that the peak power exceeds 20 μW. The average power taken over all the pulses in figure 3 a) is about 0.1 μW. The electrical energy associated with one current pulse can be calculated by integrating over the power, $\int P(t)dt$, and is found to be of the order of 0.1 μJ for R_L=50 MΩ. Figure 3 b) shows the instantaneous electrical power as a function of time from the piezoelectric device connected to a R_L=2

MΩ load when water droplets of volume 50 μL were released from h=57 cm. Here the peak power is about 1 μW, and the average energy per pulse 0.01 μJ.

3. The electrical output power depends on impact position

A factor that very clearly distinguishes the piezoelectric and contact electric devices is the signal response as a function of the impact position x of the droplet. The position x is defined as zero when the rim of the droplet just barely comes in contact with the FEP-film of the device. For a given time-dependent current pulse I(t), the energy generated in the load resistor R_L over a time interval T is given by

$$E_T = R_L \int_0^T I^2(t)dt \quad , \quad (1)$$

such that the average power or energy generated per time is $E_X=E_T/T$.

3.1 Contact charge power

Figure 4 shows the energy per second calculated using equation (1) when a 50 μL water droplet impacts from h = 5 cm and generates electrical energy through contact electrification into a 50 MΩ load resistance (a) and simultaneously also generates energy through piezoelectricity into a load resistor of 2 MΩ (b). These two load resistance values were selected for consistency with figure 3 and for easier visual comparison with data that are to be presented later in the manuscript. However, note that choosing other load resistances is not expected to alter the behavior as seen in figure 4. The total energy E_T is taken over T = 12 s, during which 19 droplets impinge on the surface. It is seen that the energy per second for the contact electric device is zero when x=0. It increases only slightly until about x = 5 mm, after which it quickly reaches something that appears as saturation. This can be explained by noting that for small x the water droplet spreads over the FEP film without contacting the aluminum film comprising the front electrode. Therefore, there is only very little or negligible charge transfer due to induction in the back-

electrode [32], and the energy transferred to the load is small. When x increases, the contact between the water and the front electrode is assured, and so the charge transfer increases as well. When x> 5 mm, the water impacts directly on top of the narrow front electrode before spreading to the FEP film. The energy transfer does not change as x increases further, since the transferred charge depends only on the water movement across the metal-dielectric barrier which for x > 5 mm remains the same. If one imagined that charge transfer would initiate only when x = 5 mm, where the impact velocity across the dielectric-metal interface is maximum, the energy should display a sharp onset as shown in the dashed line of figure 4 a). Clearly, the edge of the water droplets reaches the front electrode even for much smaller x. Moreover, the impact and spreading behavior is not identical for every incidence. This causes the observed gradual onset with corresponding large fluctuations in energy per time as observed in figure 4 a). A detailed theory to account for these observations would require an in-depth study of the droplet hydrodynamics outside the scope of this work.

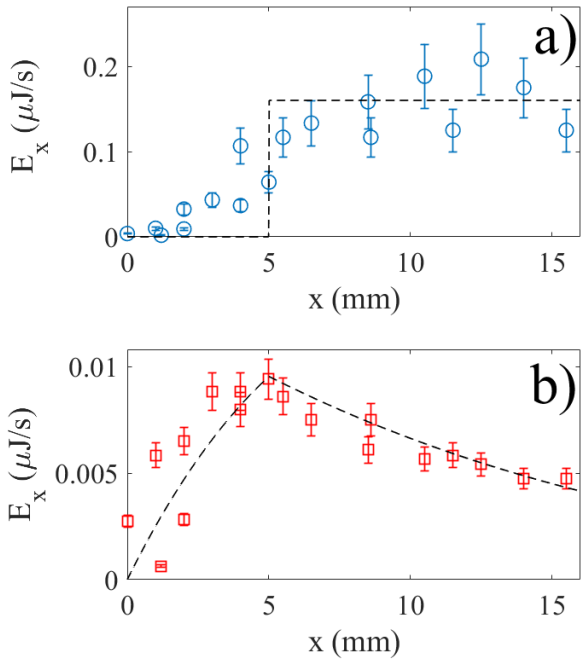

Figure 4. Energy per second due to contact electrification into 50 MΩ load resistance (a) and piezoelectricity into 2 MΩ (b). In a) the dashed line corresponds to a 'hard' onset at x = 5 mm. In b) the dashed line corresponds to a fit of equation (2) to the experimental data.

3.2 Piezoelectric power

The energy per time for the piezoelectric device shown in figure 4 b) clearly differs from that of the contact electric device in figure 4 a). While the latter provides a nearly constant energy when x > 5mm, the piezoelectric energy gradually decreases with increasing x > 5 mm. The particular geometry of the thin layer film system considered render a solution to this piezoelectromechanic problem complex, but a simple scaling relationship might provide insight. To this end, assume a small displacement y from equilibrium. Then the bending moment on the cantilever is given $M=EId^2y/dx^2$, where E is Youngs modulus and I is the section moment [88]. Assuming that the water drop applies a constant time-averaged force F on the cantilever a distance x from its edge, the bending moment is F(L-x+R), since the distance from the fixation to the water-solid interface is given by L-x and it is assumed that the force acts in the center of the drop. A simple scaling of the differential equation for the bending moment then suggests that the vertical displacement from equilibrium is $\delta=F(L-x+R)^3/EI$ [89]. Since the generated charge due to the piezoelectric effect is proportional to the displacement, it is reasonable to assume that the charge is proportional to δ, and the gathered energy is proportional to δ^2. One should also take into account that when the impact position x is smaller than the drop size diameter, parts of the droplet will end outside the cantilever. The impact dynamics is complex, but a simple approach would be to assume that the energy transferred to the piezoelectric cantilever is proportional to the ratio x/x_d, where $x_d \approx 5$ mm is the position where the entire droplet (of diameter about 5 mm) is over the FEP surface. The impact is assumed to be such that when x=0 no kinetic energy is transferred and when $x = x_d = 5$ mm the entire kinetic energy is transferred to the cantilever. The total energy transferred to the load resistor can therefore be approximated by

$$E_x = \begin{cases} k\frac{x}{x_d}(L-x+R)^6, & 0 < x \le x_d \\ k(L-x+R)^6, & x \ge x_d \end{cases} . \qquad (2)$$

The dashed line in figure 4 b) is a fit of equation (2) to the experimental data with L+R=90 mm and $k=2.5\cdot10^4$ Jm^{-6}. With these values, the fit is reasonable and may suggest that the model is adequate. However, note that the actual value of the beam length is L=40 mm, while R is about 2.3 mm, which would suggest that L+R=42.3 mm. Choosing this value of L+R in equation (2) predicts a faster decay for x > 5 mm than is observed experimentally, which may suggest that the displacement changes more slowly with impact position than suggested by the simple scaling argument giving $\delta=F(L-x)^3/EI$. This is not surprising, since the drop spreads to a finite area on the device and therefore does not provide a point force as assumed. Moreover, the aluminum front-electrode does stiffen the film in an inhomogeneous manner. However, further detailed modelling of the elastic problem is outside the scope of this work.

4. Peak current versus droplet fall height

Based on the considerations in the previous section, the droplets were released to impact at x ≈ 5 mm in the following experiments. Experimentally, the droplets were observed not impact in the same manner every time, in particular for fall heights larger than 20 cm. However, attempts were made to keep these fluctuations well below 1 mm to minimize uncertainty due to lateral position-induced fluctuations in electrical signal. It was found that the peak current I_p varies with drop impact height h in different manners for the two current generating mechanisms, as shown in figure 2 c). While the peak current due to contact charge transfer hardly increased for heights above h = 10 cm, the piezoelectric peak current continued to grow monotonously with drop release height which in the current experimental setup was limited to h = 90 cm. Different mechanisms are responsible for this behavior, since the contact electric device relies on water spreading along the dielectric-metal surface whereas the piezoelectric device relies on impact forces perpendicular to these.

4.1 Contact charge current

In the case of the contact charge device, the current is determined by the charge density σ and surface area A, such that the transferred charge is q=σA. The corresponding current is therefore

$$I = \sigma \frac{dA}{dt} + A \frac{d\sigma}{dt} \quad . \tag{3}$$

The relative change in surface charge density is usually smaller than the change in contact area with time [31,32], and it is therefore reasonable to assume that $I \approx \sigma dA/dt$. If one also assumes volume conservation, the droplet volume is constant and approximately scaling as $V_D \approx A(t)w(t)$, where A(t) is the cross-sectional area and w(t) is the time-dependent the height of the droplet during impact. The change in area is therefore $dA/dt \approx -(V_D/w^2)(dw/dt)$. If one further makes the assumption that the water drop does not change too much in extension and shape during impact, one may set $dA/dt \approx -w_{eff}(dw/dt)$, where w_{eff} is a measure of the average extension of the drop during impact. During the first part of a regular, non-splashing droplet impact it is observed in experimental data that the droplet radius increases roughly linearly with time [90]. Furthermore, one may also approximate $dw/dt \approx v_{fall}$. Assuming a constant charge density during impact, one may obtain a simple scaling for the peak current generated as

$$|I_p| = \left|\sigma \left(\frac{dA}{dt}\right)_{max}\right| \approx \sigma w_{eff} v_{fall} \quad . \tag{4}$$

Thus, the assumptions above suggest that that the current peak scales with the impact velocity. The impact velocity has been shown to be related to the height according to

$$v_{fall} = \sqrt{\frac{g}{A}(1 - e^{-2Ah})} \quad , \tag{5}$$

where g is the gravitational acceleration and $A = 3C_d\rho_{air}/8R\rho_{drop}$ [91]. Here C_d=0.796, the density of air is ρ_{air}=1 kg/m^3, the density of water is ρ_{drop}=1000 kg/m^3 and the droplet radius is R=2.3 mm. The simple model proposed here therefore suggests that the peak current is given by

$$\left|I_p\right| \approx \sigma w_{eff}\sqrt{\frac{g}{A}(1-e^{-2Ah})} \quad . \qquad (6)$$

The blue dashed line in figure 2 c) shows a fit of equation (6) to the experimental data with the numerical values listed above and $\sigma w_{eff} = 5 \cdot 10^{-7}$ C/m. If one estimates $w_{eff} = 0.01$ m to be the largest possible spreading of the droplet of impact, the surface charge density is $\sigma = 50$ μC/m^2. The theoretical fit provides a reasonable overlap with the experimental data, although the resulting value of the surface charge density is higher than in previous publications on the same material [42].

4.2 Piezoelectric current

It is seen from figure 2 c) that the piezoelectric peak current initially increases more slowly with droplet release height than the contact electric current, but the peak current increases to higher values for larger release heights. To understand this, one needs to first determine how the cantilever deflects upon drop impact. Previous research has demonstrated that the deflection δ of the cantilever beam is proportional to the velocity of the drop v_{fall} [89,92,93], consistent with an argument where the kinetic energy of the water is transformed into potential spring energy in the cantilever. Let us therefore assume that the charge q_{piezo} developed in the piezoelectric device during impact is proportional to the deflection δ. The droplet is squeezed and obtains a height b<2R, and this process takes an average time interval

$$t_{drop} = \frac{R-\frac{b}{2}}{v_{fall}} \quad . \qquad (7)$$

One may now balance inertial and capillary forces, i.e. $\rho dv/dt \approx \gamma/b^2$, where ρ is the water mass density and γ is the surface tension. Since $dv/dt \approx v_{fall}/t_{drop}$, one can estimate

$$b = (\gamma/4\rho v_{fall}^2)\left(\sqrt{1+8We}-1\right) \quad , \qquad (8)$$

where the Weber number is $We=\rho v_{fall}^2 D/\gamma$. For small Weber numbers one obtains $b \approx D=2R$, and the droplet is not compressed at all. However, this contradicts observations, since the finite contact angle (interfacial tension), among other things, is not accounted for. If the release height is very small (the velocity is small), the droplet will sit on the FEP surface and quickly assume equilibrium with a static contact angle $\theta \approx 110^{\circ}$, which means that $b \approx R$. The cantilever may still bend a small amount, often enough for the water drop to gently slide off the FEP. If on the other hand the release height is large (the velocity is large), the droplet is compressed upon impact and subsequently bounces away. While experimental investigations have revealed a much more complex picture for droplets impacting a cantilever surface [89,90], the simple scaling approach used here allows for simple analytical formulas to provide insight into the peak current. The balancing of capillary and inertial forces using equation now results in

$$b = (\gamma/4\rho v_{fall}^2)\left(\sqrt{1+8We}-1\right) \approx (1/v_{fall})\sqrt{\gamma R/\rho} \text{ if } We \gg 1 \quad . \qquad (9)$$

The compression of the water drop increases with velocity. However, it is seen that $b \ll R$ when $v>0.5$ m/s (corresponding to $h > 2$ cm) since $\sqrt{\gamma R/\rho} \approx 4 \cdot 10^{-4} \mathrm{s/m}$. Thus, it is a reasonable assumption to put $t_{drop} \approx R/v_{fall}$ under all circumstances considered here, which means that the peak current generated can be estimated to be

$$|I_p| \approx \frac{q_{piezo}}{t_{drop}} \approx c v_{fall}^2 = c\frac{g}{A}\left(1-e^{-2Ah}\right) \quad , \qquad (10)$$

where c is a constant. The red dashed line in figure 2 c) is a fit of equation (10) to the experimental data with $c = 2 \cdot 10^{-7}$ Cs/m^2. It is noted that a fit of the square of the velocity to the experimental data for the piezoelectric device is better than a fit assuming linearity between current and drop velocity, thus distinguishing the behavior of the piezo device from that of the contact electric device.

5. The electrical current in presence of cantilever vibrations

The investigations reported above were all based on a stationary energy harvesting device impacted by moving water droplets. However, in many circumstances one could imagine that the device is vibrating periodically. For example, a cantilever may vibrate in presence of a vibrating mechanical structure or flutter in presence of wind. To this end, it is therefore of interest to gain knowledge of the electrical output of the device under such conditions. As examples of such measurements, figure 5 shows the measured velocity of the vibrating device (a), the short circuit current due to contact electrification (b) as well as the piezoelectric short circuit current (c).

Initially, the electromagnetic shaker is turned off, and 50 μL water droplets impinge the device from a height of h = 2 cm. This results in current peaks of about 0.2 μA from the contact electrification and 0.1 μA from piezoelectricity. After about 6 seconds the electromagnetic shaker is turned on, and it is seen that the velocity fluctuates periodically at a frequency of f = 4 Hz with peak velocity values of about 0.12 m/s. The current due to contact electrification start to fluctuate in a manner that does not resemble the velocity variations, with peak values from 0.1 μA to 0.3 μA. On the other hand, the piezoelectric fluctuations in the short circuit current resemble those of the velocity fluctuations with peak values of about 0.4 μA.

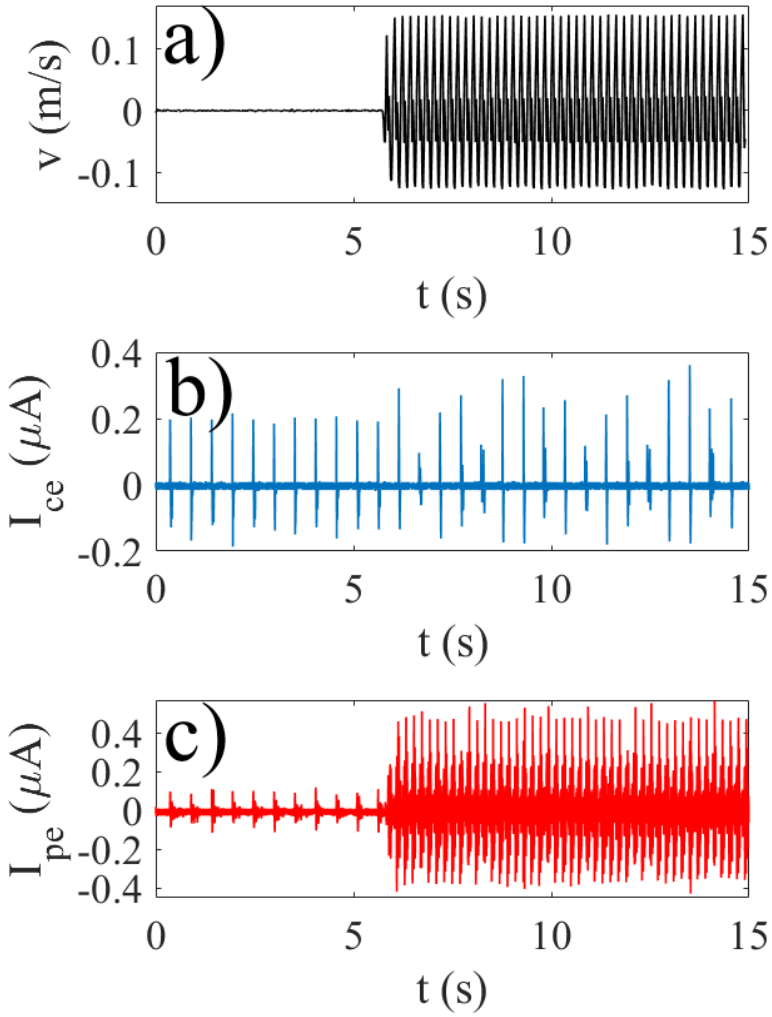

Figure 5. The electromagnetic shaker is turned on to vibrate at 4 Hz after about 6 seconds, and a) shows the variations in velocity, b) the variations in the short circuit current due to contact electrification and c) the variations in the short circuit current from the piezoelectric mechanism. The 50 μL water droplets were released from a height of h = 2 cm.

A simple model can be considered to understand the contact electric currents observed in figure 5 b). It is noted that the water droplets approach the vibrating cantilever with a vertical velocity

$$v_{drop}(t) = v_{fall} + v(t) = v_{fall} + v_1 \sin(2\pi f t) \quad , \quad (11)$$

where v_{fall} is the velocity due to the fall at the moment of impact and $v=v_1\sin(2\pi ft)$ is the time-dependent cantilever velocity. Assuming a constant charge density and the considerations in the previous section, the current generated is proportional to the velocity such that

$$I_{ce} \approx \sigma \frac{dA}{dt} \approx -\sigma w_{eff} v_{fall} \left[1 + \frac{v(t)}{v_{fall}}\right] \quad . \quad (12)$$

Let $I_{c0}(t)=-\sigma w_{eff} v_{fall}$ be the current in absence of cantilever vibrations. Assume for simplicity that the contact electric signal consists of a sum of positive and a negative gaussian pulses displaced by t_1 with respect to each other, and repeated at intervals t_0, such that

$$I_{c0}(t) = I_A \sum_{m=1}^{m=N} e^{-(t-mt_0)^2} - I_B \sum_{m=1}^{m=N} e^{-(t-mt_0-t_1)^2} \quad . \quad (13)$$

Comparison with figure 2 a) suggests that the two current amplitudes are related as $I_B=0.8I_A$, and that $t_1=0.02$ s. While it is seen from figure 2 a) that the current pulses do not look exactly like a bi-gaussian pulse and a model based on equation (13) therefore cannot provide quantitative accuracy, it does provide a qualitative toy model which is helpful when trying to understand the temporal variations in current when the cantilever vibrates. For a given vibration frequency, the contact electric signal is modulated by a factor such that the total signal becomes

$$I_{ce}(t) = I_{c0}[1 + b\sin(2\pi ft)] \quad , \quad (14)$$

where $b = v_1/v_{fall}$, i.e. the ratio between the maximum cantilever velocity and the velocity of the droplet in absence of vibrations. It was observed experimentally that small changes in vibration frequency would result in large variations in the sequence with which different peak values would occur. For example, if the vibration frequency of the cantilever f is a multiple of the water dropping frequency $f_0=1/t_0$, one would expect all the pulses to be the same with the same peak current. However, a small change in vibration frequency would lead to a modulation governed by the difference $\Delta f=f-f_0$. As an example of how small changes in vibration frequency changes the current fluctuations drastically, figure 6 shows the contact electric current when f=4.15 Hz (a) and f=4.35 Hz (b) with a drop frequency of $f_0=1/t_0=1$ Hz and b=0.3.

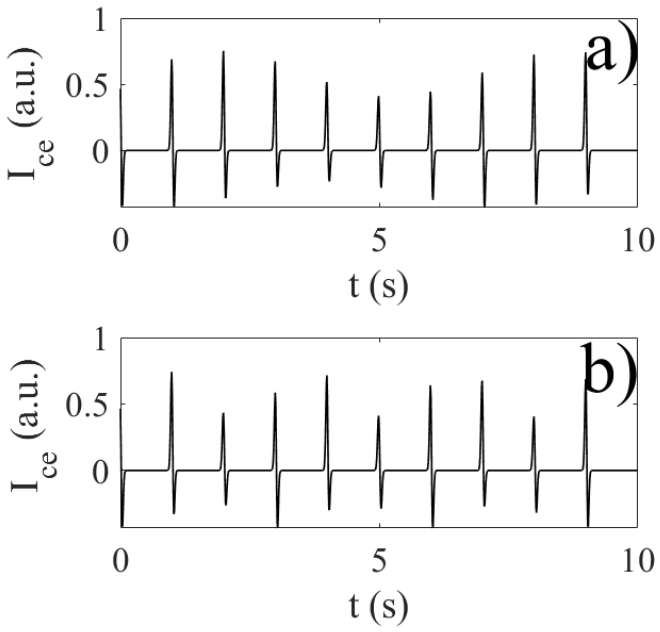

Figure 6. Simulation of contact charge current versus time for a drop frequency f_0 = 1 Hz and cantilever frequency f=4.15 Hz (a) and f=4.35 Hz (b).

Similar considerations can be made for the piezoelectric signal, but one should remember that piezoelectricity generates current directly from the vibrations in addition to the droplet impact. Based on the discussion above, it is reasonable to assume that the current is proportional to the velocity squared,

$$I_{pe}(t) \approx cv_{drop}^2 + I_v = cv_{fall}^2\left[1 + \frac{v(t)}{v_{fall}}\right]^2 + I_v \quad , \qquad (15)$$

where the latter term (I_v) accounts for the current generated in absence of any water droplets. Since the charge generated in the piezoelectric material is proportional to the cantilever deflection δ, one may assume that I_v=pv, where p is a constant. In presence of impacting water droplets, the smallest fall height is h = 2 cm, corresponding to $v_{fall} \approx 0.5$ m/s, and the largest cantilever vibration velocity is $v_1 = 0.25$ m/s. If one lets $I_{pe0}= cv_{fall}^2$ and $b = v_1/v_{fall}$ the piezoelectric signal can be written on the form

$$I_{pe}(t) = I_{pe0}[1 + b\sin(2\pi ft)]^2 + I_v \quad . \qquad (16)$$

If $pv_1 >> cv_{fall}^2$, the droplet-independent current dominates, as is seen for t> 6 s in figure 5 c). For t < 6 s the fall velocity is sufficiently large that $pv_1 << cv_{fall}^2$.

6. Energy harvesting versus cantilever velocity

In energy harvesting, one is most often interested in the energy that is accumulated over time. To obtain a measure of this, the electrical energy delivered per second by contact electricity and piezoelectricity into

loads of 50 MΩ and 2 MΩ, respectively, was recorded as function of the peak velocity v_1 when the droplets impacted the device at x = 5 mm. The energy per second E_s, also called average power, related to contact electrification is shown in figure 7 a) for drop release heights h = 2 cm (red circles), h = 20 cm (black circles) and h = 57 cm (blue circles). The water droplets impact the FEP surface at a rate of 1.5 drops per second, and the averaging is taken over 10-12 seconds. It is found that averaging over 3-4 droplets normally gives stable average values that do not change with time for a given drop rate. For h = 2 cm the electrical power increases by a factor of 5 as the peak vibration velocity changes from zero to 0.25 m/s. For heights h > 10 cm or above, the harvested electric power appears to decrease weakly with increasing velocity. However, taking into account uncertainty it is seen that this decline is within the error bars, and one can therefore only conclude that the harvested power does not change significantly with cantilever velocity when h > 10 cm. According to the equation $I \approx \sigma dA/dt$ the current, and therefore also the electrical power, depends on the change in area per time interval. For sufficiently large velocities it is likely that the droplet collides with the FEP surface in an irregular and splashing manner that does not give rise to a linear increase in dA/dt with relative droplet velocity. Instead, it appears that dA/dt remains nearly constant, thus giving rise to a nearly constant harvested power as well. However, at low release heights such as h = 2 cm, the electrical power increases with cantilever vibration velocity, and will therefore be analyzed more carefully in the following.

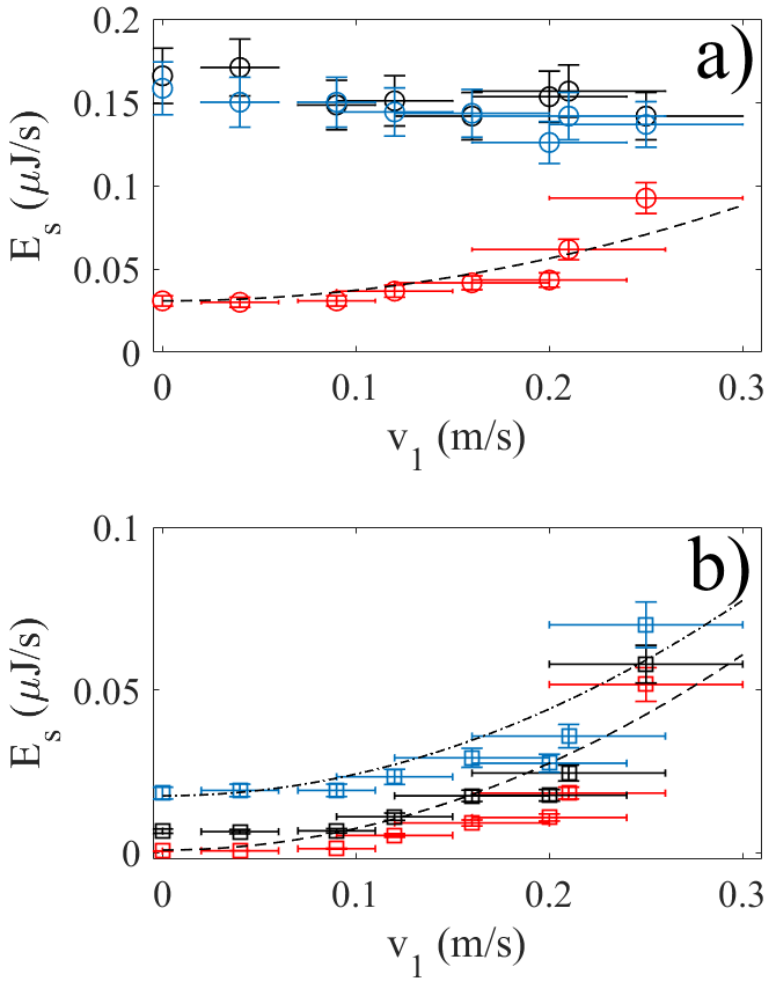

Figure 7. The average power due to contact electrification into 50 MΩ load resistance (a) and piezoelectricity into 2 MΩ (b) for h=2 cm (red circles and squares), h=20 cm (black circles and squares) and h=57 cm (blue circles and squares). In a) the dashed line is a fit of equation (22) to the experimental data, whereas in b) the dashed and dash-dotted lines are fits of equation (23) to the experimental data.

To explain the observed behavior for h = 2 cm, one could first consider the instantaneous power given by $P(t)=R_L I^2(t)$, or

$$P(t) = R_L I_0^2(t)[1 + 2b\sin(2\pi ft) + b^2\sin^2(2\pi ft)] \quad . \qquad (17)$$

The energy integrated over a single pulse of time interval T_{pulse} is

$$E_1(t) = \int_0^{T_{pulse}} P(t)\,dt \quad . \quad (18)$$

Since the duration of a pulse (T_{pulse} < 0.1 s) is smaller than any cantilever frequency considered in this work, one may assume that the pulse picks out the cantilever phase at a given moment in time and therefore approximate the pulse energy as

$$E_1(t) \approx [1 + 2b\sin(2\pi ft) + b^2\sin^2(2\pi ft)] \int_0^{T_{pulse}} R_L I_0^2(t)dt \quad . \quad (19)$$

The latter integral is just the energy E_{drop} generated by one droplet in absence of cantilever vibrations, i.e.

$$E_{drop} = R_L \int_0^{T_{pulse}} I_0^2(t)dt \quad . \quad (20)$$

Clearly, $E_1(t)$ depends on the chosen phase (frequency) of the cantilever, and is as such not so interesting from the perspective of energy harvesting. If one takes the average over a large time T interval covering many pulses, the total energy becomes

$$E_T \approx \frac{E_{drop}}{T}\int_0^T [1 + 2b\sin(2\pi ft) + b^2\sin^2(2\pi ft)]dt = P_{drop}\left(1 + \frac{b^2}{2}\right) \quad . \quad (21)$$

where the average power per drop is $P_{drop}=E_{drop}/T$. The average power, or energy per time interval extending many impacting water droplets, is given as

$$E_s(t) \approx P_{drop}(1 + b_a^2) \quad , \tag{22}$$

where $b_a = b/\sqrt{2}$. The black, dashed line in figure 7 a) shows a fit of equation (22) to the experimental data with P_{drop} =0.031 μJ/s and b_a=4.6v_1. In each of the data points, the averaging is done over 12 seconds, corresponding to more than 15 droplets. If one assumes that b = v_1/v_{fall}, the fit seems to suggest that v_{fall} ≈ 0.2 m/s, which is smaller than the actual velocity that droplets had upon impact. It should however be pointed out that the uncertainty in velocity measurement data in figure 7 a) are large due to the limited precision of the available ultrasonic measurement system.

The average energy per time is shown in figure 7 b) for the piezoelectric signal for drop release heights h = 2 cm (red squares), h = 20 cm (black squares) and h = 57 cm (blue squares). When f=0 Hz, it is observed that the energy per time increases with release height. It is also observed that the energy increases with cantilever vibration velocity v for all release heights. If one linearizes equation (16), one may to the simplest approximation obtain

$$E_s(t) \approx P_{drop}(1 + g^* v^2) \quad , \tag{23}$$

where P_{drop} is the average power per drop in absence of vibrations and g* is a fitting constant. It is ensured that the expression for E_s versus velocity is on the same form as in equation (22) as long as the linear term due to I_v in the latter dominates the contribution from the vibrating cantilever. The dashed line of figure 7 b) is a fit of this equation to the experimental data with E_{s0}=0.83 nJ/s and g*=800 s^2/m^2, and the dash-dotted line is a fit with E_{s0}=0.018 μJ/s and g*=38 s^2/m^2. In both cases it is seen without doubt that E_s is not linear in velocity and that it is increasing in a fashion that depends on both the vibration velocity and drop release height.

7. Average power versus load resistance

From the data of power versus time in figure 3, one can extract the average power E_s for different load resistances. The power data such as those in figure 3 were gathered for about 10 s for 50 µL water droplets impinging at a rate of about 1.5 drop per second. Examples of the average power as a function of load resistance is shown as red circles for contact electrification in figure 8 a) and as red squares for the piezoelectricity in figure 8 b).

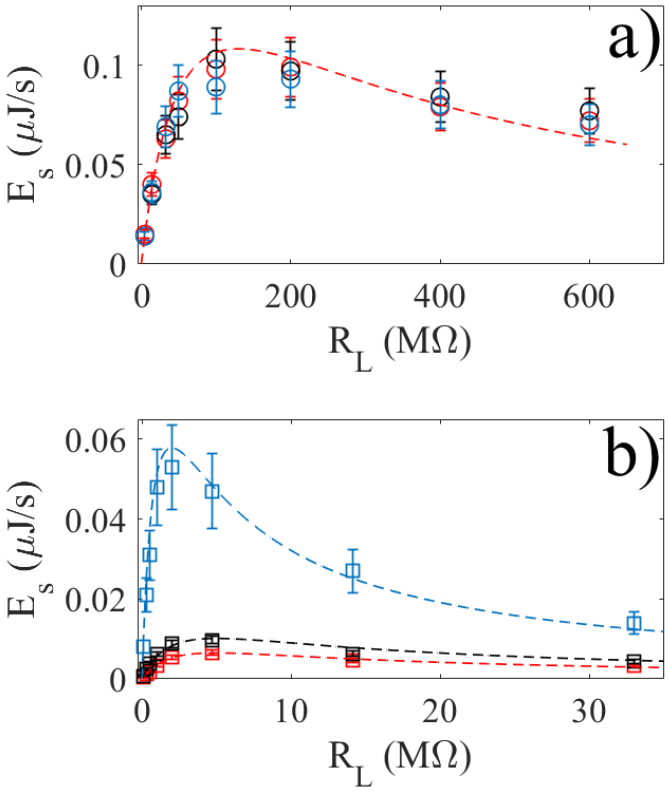

Figure 8. The average power due to contact charge transfer (a) and piezoelectricity (b) as a function of load resistance for f=0 Hz cm (red circles and squares), f=4 Hz (black circles and squares) and f=8 Hz (blue circles and squares). The 50 µL water drops were released from a height of h=10 cm. The dashed red line in a) is a fit of equation (25) to the experimental data. The dashed lines in b) are fits of equation (25) to the experimental data for the different vibration frequencies. See text for details.

The average electrical power though the load resistors was also measured for vibration frequencies f = 4 Hz (black circles and squares) and f = 8 Hz (blue circles and squares), corresponding to peak vibration velocities of 0.12 m/s and 0.25 m/s, respectively.

For the contact electrification, a maximum average electrical power transfer of about 0.1 μW is achieved for a load resistance of about 100 MΩ at this particular volume rate. However, it should also be pointed out that the average electrical power does not change much when altering the power between 50 MΩ and 200 MΩ. It is seen from figure 8 a) that the average power due to contact electrification does not depend, to within the uncertainty, on the vibration velocities or frequencies considered here. The reason for this is that the water drops are falling from a height at h = 10 cm, for which the contact charge transfer has already reached a stagnation as also corroborated by the data in figures 2 c) and 7 a).

The data for the average power versus load resistance in figure 8 a) can be modelled by noting that the current through the load is

$$I_t = \frac{f(t)U_0}{R_L+R_i} \quad , \tag{24}$$

where U_0 is the voltage in absence of load, R_i is the internal resistance of the triboelectric generator and f(t) is a time-dependent function that resembles the current of figure 2 and therefore determines the pulse shape of the current. The time-averaged power is given by

$$E_s = R_L\left[\frac{U_0^*}{(R_L+R_i)}\right]^2 \quad , \qquad U_0^* = (U_0/T)\int_0^T f^2(t)dt \quad . \tag{25}$$

A fit of this equation with U_0^*=7.5 V and R_i=130 MΩ is shown as a red, dashed line in figure 8 a). Note that the overlap between the experimental data and the theoretical expression is acceptable to within the uncertainty, suggesting that the functional dependency is correctly modelled. However, it should also be pointed out that although U_0^* is an effective voltage that depends on the current pulse-shape, it is in most cases approximately equal to the open circuit voltage.

The measured average power as a function of load resistance for the piezoelectric signal is shown in figure 8 b) for f = 0 Hz cm (red squares), f = 4 Hz (black squares) and f = 8 Hz (blue squares). Figure 8 b) clearly demonstrates that the average electrical power increases significantly when the vibration frequency (and velocity) is increased, from a maximum of 0.01 μW at f = 0 Hz to 0.06 μW at f = 8 Hz. In a similar manner as for the contact charge transfer, the average piezoelectric power can be modelled using equation (25). The red-dashed line fits the data for f = 0 Hz with U_0^*=0.36 V and R_i=5 MΩ, the black-dashed line fits the data for f = 4 Hz with U_0^*=0.45 V and R_i=5 MΩ, while the blue-dashed line fits the data for f = 8 Hz with U_0^*=0.68 V and R_i=2 MΩ. In all cases the fit is acceptable taking into account uncertainty. It is also noted that the internal resistance decreases from 5 MΩ to 2 MΩ as the frequency increases from 4 Hz to 8 Hz. The uncertainty is rather large for load resistances between 5 MΩ and 2 MΩ where the average power peaks are found, and the average electrical power does not change much in this region. This justifies the use of a load resistance of 2 MΩ when finding E_s in the previous sections. It should also be pointed out that the fitted curves in figure 8 are useful for demonstrating that both the charge generating mechanisms can be well modelled as electric generators with resistive internal loads, and for determining the load that allows extraction of most average power.

8. Energy output versus water flow rate

The amount of electrical energy deposited in the load resistor was found to depend on the volume rate of the water droplets, as shown in figure 9. Here it should be mentioned that volume rate corresponds to dropping frequency. For reference, note that one droplet has volume 50 μL, which means that a droplet frequency of one droplet per second corresponds to a volume rate of 0.05 mL/s.

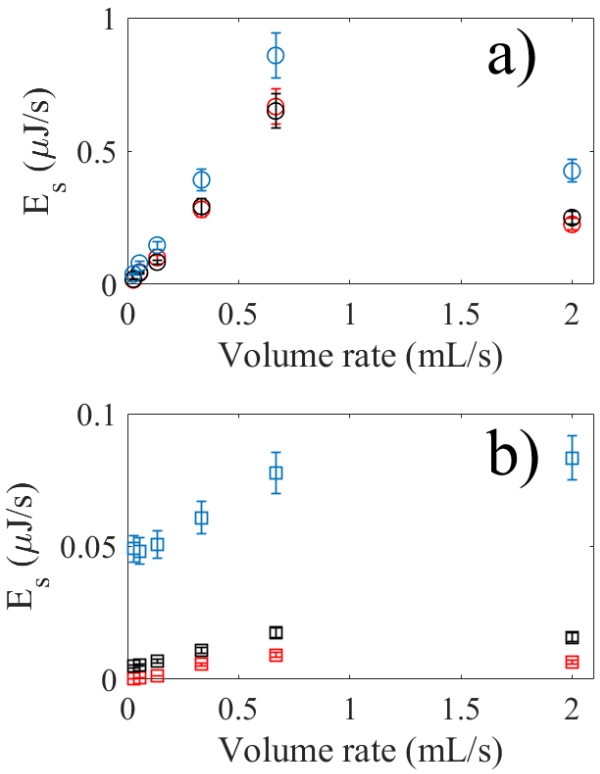

Figure 9. Average power for the contact charge transfer into 50 MΩ load resistance (a) and piezoelectric generator into 2 MΩ (b) for f=0 Hz cm (red circles and squares), f=4 Hz (black circles and squares) and f=8 Hz (blue circles and squares). The water was released from a height of h=5 cm.

In figure 9 a), the red circles the energy per second due to contact charge transfer with a 50 MΩ load resistance is visualized for volume rates up to 2 mL/s, which is the maximum of the current setup. The water was released from a height of h=5 cm. It is seen that the electrical energy increases linearly with

volume flow rate up to about 0.7 mL/s, above which a continuous flow sets in such that the water does not break up into droplets. At 2 mL/s the energy has decreased significantly.

The decrease in energy above the transition to a continuously flowing film can be explained as due to the lack of discontinuous surface needed to transfer charge, as was also noted in Refs. [32,33]. This observation agrees with the conclusions of refs. [32,33], and is found to have rather general validity for various type of triboelectric generators based on either front or back-type electrode. The black and blue circles in figure 9 a) is the energy per time interval obtained when the electromagnetic shaker is set into oscillations at 4 Hz and 8 Hz, respectively. It is seen that the energy transferred to the 50 MΩ load increases slightly when using 8 Hz oscillations corresponding to peak velocities of 0.25 m/s. However, the increase in transferred energy is small since h= 5 cm corresponds to a height were the currents starts to flat out as seen in figure 2 c).

The red squares in figure 9 b) show the energy per time interval from the piezoelectric signal into a load resistor of 2 MΩ for a water release height of h= 5 cm as the volume rate is varied. The black squares correspond to f=4 Hz (with peak velocity 0.12 m/s) and the blue squares to f=8 Hz (corresponding to peak velocity 0.25 m/s). It is seen that in all cases, the energy delivered to the load reaches a maximum (to within the uncertainty) once a continuous flow of water is obtained above 0.7 mL/s. Thus, the output of the piezoelectric device does not drastically reduce its performance above this continuous flow transition. On the other hand, it is seen that the energy delivered increases drastically when the cantilever oscillations are initiated, with a fivefold increase in power following a doubling in peak velocity.

The main qualitative results related to harvestable electrical power found in this work are summarized in table 1. These factors should be considered when optimizing the design of combined energy harvesting systems for use with both forced oscillations due to e.g. wind as well as impacts dues to water droplets.

Average power depends on	***Contact electricity***	***Piezoelectricity***
Impact position	Depends on impact position	Depends on impact position
Impact velocity (v)	Increases with v^2 at small velocities, saturates at larger velocities	Increases with v^2
Volume rate	Increases strongly with volume rate until a continuous water film form	Increases weakly with volume rate

Table 1. Qualitative summary of main findings in this work.

9. Conclusion

The aim of this work was to investigate how an energy harvesting unit utilizing both contact charge transfer and the piezoelectric effect simultaneously would behave when exposed to both vibrations as well as impact forces due to falling water droplets. It was found that the contact charge transfer and piezoelectric signals were rather different, although they exhibited similar energy versus velocity signature for small water droplet impact heights. The impact position of the water droplet played a role in the energy harvesting and had to be optimized. Both the contact charge and piezoelectric generators could be modelled exhibiting resistive internal loads thus featuring an external load corresponding to optimal power output.

The proposed device may have applications as small-scale water droplet impact energy harvesters exposed to fluctuations due to wind or vibrating infrastructure. For example, one could imagine placing a large

field of such devices in a location where the wind forces them into sinusoidal oscillations while water droplets from rain are hammering down. As shown in this work, under ideal conditions there may be a contribution from both the wind and rain to the harvested energy. However, this requires that the water droplets impact on the active area perpendicular to oscillations. Currently, the optimal position for water droplet impact is narrow, but one could imagine increasing it using a front-electrode composed of a thin metallic wire that extends in a serpent formation across the hydrophobic polymer surface.

Due to the small amount of energy harvested by such a small device, it is most likely to have applications for powering small sensors. To this end, one could also imagine it for use as self-powered environmental sensors that allow one to distinguish between local wind guests and water droplet impacts. However, such applications would require more testing of the device under conditions were the water droplets and wind comes from more than a single direction. Dual beams [94], twisted piezoelectric beams [95] and optimized tilted bluff bodies [96] have been developed to improve energy harvesting from multiple directions. Future work could try to combine such approaches with a contact electricity device also designed for multiple impact directions. Another direction would be to improve the energy harvesting capabilities by introducing water collection mechanisms as those discussed in Refs. [78,97].

REFERENCES

(1) M. Umeda, K. Nakamura and S. Ueha, "Analysis of the transformation of mechanical impact energy to electric energy using piezoelectric vibrator", Jap. J. Appl. Phys., **1996**, 35, 3267.

(2) N.M. White, P. Glynne-Jones and S.P. Beeby, "A novel thick-film piezoelectric micro-generator", Smart Mater. Struct. **2001**, 10, 850.

(3) H. Elahi, M. Eugeni and P. Gaudenzi, "A review on mechanisms for piezoelectric-based energy harvesters", Energies, **2018**, 11, 1850.

(4) N. Wu, B. Bao and Q. Wang, "Review on engineering structural designs for efficient piezoelectric harvesting to obtain high power output", Engineering Structures, **2021**, 235, 112068.

(5) M. Iqbal, M.M. Nauman, F.U. Khan, P.E. Abas, Q. Cheok, A. Iqbal and B. Aissa, "Vibration-based piezoelectric, electromagnetic, and hybrid energy harvesters for microsystems applications: A contributed review", Int. J. Energy Res., **2020**, 1-38,

(6) H.A. Sodano, D.J. Inman and G. Park, "Comparison of piezoelectric energy harvesting devices for recharging batteries", J. Int. Mat. Syst. Struct., **2005**, 16, 799-807.

(7) H.D. Akaydin, N. Elvin and Y. Andreopoulos, "Wake of a cylinder: a paradigm for energy harvesting with piezoelectric materials", Experiments in Fluids, **2010**, 49, 291-304.

(8) D.A. Wang and H.H. Ko, "Piezoelectric energy harvesting from flow-induced vibration", Journal of Micromechanics and Microengineering, **2010**, 20, 025019.

(9) J. Wang, D. Yurchenko, G. Hu, L. Zhao, L. Tang and Y. Yang, "Perspectives in flow-induced vibration energy harvesting", Appl. Phys. Lett., **2021**, 119, 100502

(10) H. Elahi, M. Eugeni, F. Fune, L. Lampani, F. Mastroddi, G.P. Romano and P. Gaudenzi, "Performance evaluation of a piezoelectric energy harvester based on flag-flutter", Micromachines, **2020**, 11, 933.

(11) R. Guigon, J.J. Chaillout, T. Jager and G. Despesse, "Harvesting raindrop energy: experimental study", Smart Mater. Struct. **2008**, 17, 015039.

(12) M.A. Ahmad, "Piezoelectric water drop energy harvesting", J. Electronic Materials, **2014**, 43, 452-458.

(13) C.H. Wong, Z. Dahari, A.A. Manaf and M.A. Miskan, "Harvesting raindrop energy with piezoelectrics: a review", J. Electronic Materials, **2015**, 44, 13-21.

(14) S.C.J. Jellard, S.H. Pui, S. Chen, K. Yao and N.M. White, "Water droplet impact energy harvesting with P(VDF-TrFE) piezoelectric cantilevers on stainless steel substrates", Smart Mater. Struct., **2019**, 28, 095002.

(15) G. Hao, X. Dong, Z. Li and X. Liu, "Dynamic response of PVDF cantilever due to droplet impact using an electromechanical model", Sensors, **2020**, 20, 5764.

(16) M.A. Ilyas and J. Swingler, "Towards a prototype module for piezoelectric energy harvesting from raindrop impacts", Energy, **2017**, 125, 716-725.

(17) F. Viola, "Comparison among different rainfall energy harvesting structures", Applied Sciences, **2018**, 8, 955.

(18) C.H. Wong, Z. Dahari, A.A. Manaf and M.A. Miskan, "Piezoelectric beam length optimization for raindrop energy harvesting application", Applied Mechanics and Materials, **2015**, 705, 247-251.

(19) S. Gart, J.E. Mates, C.M. Megaridis and S. Jung, "Droplet impacting a cantilever: A leaf-raindrop system", Phys. Rev. Appl., **2015**, 3, 044019.

(20) A. Doria, G. Fanti, G. Filipi and F. Moro, "Development of a novel piezoelectric harvester excited by raindrops", Sensors, **2019**, 19, 3653.

(21) W. Thomson, "On a self-acting apparatus for multiplying and maintain electric charges, with applications to illustrate the voltaic theory", Proc. R. Soc. London, **1867**, 16, 67-72, available at http://www.jstor.org/stable/112474.

(22) I. Langmuir, "Surface electrification due to recession of aqueous solutions from hydrophobic surfaces", J. Am. Chem. Soc., **1938**, 60, 1190-1194

(23) M. Matsui, N. Murasaki, K. Fujibayashi, P.Y. Bao and Y. Kishimoto, "Electrification of pure water flowing down a through set up with a resin sheet", J. Electrostatics, **1993**, 31, 1-10.

(24) K. Yatsuzuka, Y. Mizuno and K. Asano, "Electrification phenomena of pure water droplets dripping and sliding on a polymer surface", J. Electrostatics, **1994**, 32, 157-171.

(25) R. Williams, "The relation between contact charge transfer and chemical donor properties", J. Coll. Int. Sci., **1982**, 88, 530-535.

(26) P.W. Chudleigh, "Mechanism of charges transfer to a polymer surface by a conducting liquid contact", J. Appl. Phys., **1976**, 47, 4475-4482.

(27) J.W. Park, Y. Yang, S.-H. Kwon and Y.S. Kim, "Influences of surface and ionic properties on electricity generation of an active transducer driven by water motion", J. Phys. Chem. Lett., **2015**, 6, 745-749.

(28) J. W. Park, S. Ong, C.H. Shin, Y.Y. Yang, S.A.L. Weber, E. Sim and Y.S. Kim, "Ion specificity on electric energy generated by flowing water droplets", Angew. Chem. Int. Ed., **2018**, 57, 2091-2095.

(29) J. Nie, Z. Ren, L. Xu, S. Lin, F. Zhan, X. Chen and Z.L. Wang, "Probing contact-electrification-induced electron and ion transfers at a liquid-solid interface", Adv. Mater., **2020**, 32, 1905696.

(30) L.E. Helseth, "Influence of salt concentration on charge transfer when a water front moves across a junction between a hydrophobic dielectric and a metal electrode", Langmuir, **2020**, 36, 8002-8008.

(31) L.E. Helseth, "The influence of microscale surface roughness on water-droplet contact electrification", Langmuir, **2019**, 35, 8268-8275.

(32) L.E. Helseth, "Electrical energy harvesting from water droplets passing a hydrophobic polymer with a metal film on its back side", J. Electrostatics, **2016**, 81, 64-70.

(33) L.E. Helseth, "Harvesting energy from light and water droplets by covering photovoltaic cells with transparent polymers", Applied Energy, **2021**, 300, 117394.

(34) L. Yang, Y. Wang, Y. Gao, W. Zhang, Z. Zhao, "Robust working mechanism of water droplet-driven triboelectric nanogenerator: Triboelectric output versus dynamic motion of water droplet", Adv. Mat. Interfaces, **2019**, 6, 1901547.

(35) A. Riaud, C. Wang, J. Zhou, W. Xu and Z. Wang, "Hydrodynamic constraints on the energy efficiency of droplet electricity generators", Microsystems & Nanoengineering, **2021**, 7, 49.

(36) D. Choi, H. Lee, D.J. Im, I.S. Kang, G. Lim, D.S. Kim and K.H. Kang, "Spontaneous electrical charging of droplets by conventional pipetting", Scientific Reports **2013**, 3, 2037.

(37) D. Choi and D. S. Kim, "A zeta-pipet tip to reduce the spontaneously induced electrical charge of a dispensed aqueous droplet", Langmuir. **2014**, 30, 6644-6648.

(38) Y. Song, B. Xu, Y. Yuan, H. Xu and D. Li, “Coalescence of a water drop with an air-liquid interface: Electric current generation and critical micelle concentration (CMC) sensing”, ACS Appl. Mater. Interfaces, **2019**, 11, 16981-16990.

(39) P. Jiang, L. Zhang, H. Guo, C. Chen, C. Wu, S. Zhang, et al., “Signal output of triboelectric nanogenerator at oil-water-solid multiphase interfaces and its application for dual-signal chemical sensing”, Adv. Mat., **2019**, 31, 1902793.

(40) J. K. Moon, J. Jeong, D. Lee, H. K. Pak, “Electrical power generation by mechanically modulating electrical double layers” Nat. Commun., **2013**, 4**,** 1487.

(41) Z.H. Lin, G. Cheng, S. Lee, K.C. Pradel, Z.L. Wang, “Harvesting water drop energy by sequential contact electrification and electrostatic induction process”, Adv. Mater., **2014**, 26, 4690-4696.

(42) L.E. Helseth, X.D. Guo, “Contact electrification and energy harvesting using periodically contacted and squeezed water droplets”, Langmuir, **2015**, 31, 3269-3276.

(43) G. Zhu, Y. Su, P. Bai, J. Chen, Q. Jing, W. Yang, et al., “Harvesting water wave energy by asymmetric screening of electrostatic charges on a nanostructured hydrophobic thin-film surface”, ACS Nano, **2014**, 8, 6031-6037.

(44) S.-H. Kwon, J. Park, W.K. Kim, Y. Yang, E. Lee, C.J. Han, et al., “An effective energy harvesting method from a natural water motion active transducer”, Energy Environ. Sci., **2014**, 7, 3279-3283.

(45) L.E. Helseth, H.Z. Wen, “Evaluation of energy generation potential of rain cells”, Energy, **2017**, 119, 472-482.

(46) Xu, M. Dong, F. Guo, X. Liu, G. Chen, et al., "Water-solid triboelectric nanogenerators: An alternative means for harvesting hydropower", Renewable and Sustainable Energy Reviews, **2019**, 115, 109366.

(47) W. Tang, B.D. Chen, Z.L. Wang, "Recent progress in power generation from water/liquid droplet interaction with solid surfaces", Advanced Functional Materials, **2019**, 29, 1901069.

(48) X. Zhang, M. Yu, Z. Ma, H. Ouyang, Y. Zou, S.L. Zhang, et al., "Self-powered distributed water level sensors based on liquid-solid triboelectric nanogenerators for ship draft detecting", Adv. Functional Mat., **2019**, 29, 1900327.

(49) Q. Shi, H. Wang, T. Wang, C.K. Lee, "Self-powered liquid triboelectric microfluidic sensor for pressure sensing and finger motion monitoring applications", Nano Energy, **2016**, 30, 450-459.

(50) G. Chen, X. Liu, S. Li, M. Dong, D. Jiang, "A droplet energy harvesting and actuation system for self-powered digital microfluidics", Lab Chip, **2018**, 18, 1026-1034.

(51) Y. Su, X. Wen, G. Zhu, J. Yang, J. Chen, P. Bai, et al., "Hybrid triboelectric nanogenerator for harvesting water wave energy and as a self-powered distress signal emitter", Nano Energy, **2014**, 9, 186-195.

(52) J. Wang, H. Zhang, X. Xie, M. Gao, W. Yang, Y. Lin, "Water energy harvesting and self-powered visible light communication based on triboelectric nanogenerator", Energy Technology, **2018**, 6, 1929-1934. h

(53) J. Wang, H. Wang, X. Li, Y. Zi, "Self-powered electrowetting optical switch driven by a triboelectric nanogenerator for wireless sensing", Nano Energy, **2019**, 66, 104140.

(54) K.R. Wijewardhana, T.Z. Shen and J.K. Song, "Energy harvesting using air bubbles on hydrophobic surfaces containing embedded charges", Applied Energy, **2017**, 206, 432-438.

(55) Q.T. Nguyen and K.K. Ahn, “Fluid-based triboelectric nanogenerators: A review of current status and applications”, Int. J. of Precis. Eng. and Manuf.-Green Tech., **2021**, 8, 1043-1060.

(56) C.P. Vo, M. Shahriar, C.D. Le, K.K. Ahn, “Mechanically active transducing element based on solid-liquid triboelectric nanogenerator for self-powered sensing”, Int. J. of Precis. Eng. and Manuf.-Green Tech., **2019**, 6, 741-749.

(57) C. Chen, Z. Wen, A. Wei, X. Xie, N. Zhai, X. Wei, et al., “Self-powered on-line ion concentration monitor in water transportation driven by triboelectric nanogenerator”, Nano Energy, **2019**, 62, 442-448.

(58) W. Zhang, P. Wang, K. Sun, C. Wang, D. Diao, “Intelligently detection and identifying liquids leakage combining triboelectric nanogenerator based self-powered sensor with machine learning”, Nano Energy, **2019**, 56, 277-285.

(59) L.E. Helseth, “A water droplet-powered sensor based on charge transfer to a flow-through front surface electrode”, Nano Energy, **2020**, 73, 104809.

(60) C. Chen, G. Xie, M. Yao, H. Pan and Y. Su, “A membrane raindrop generator and its application as a self-powered pH sensor”, Micro Nano Lett., **2021**, 16, 51-57.

(61) Y.P. Pao, C.C. Yu, Y.Z. Lin, S. Chatterjee, S. Saha, N. Tiwari, et al., “Carbohydrate-protein interactions studied by solid-liquid contact electrification and its use for label-free bacterial detection”, Nano Energy, **2021**, 85, 106008.

(62) S. Jang, M. La, S. Cho, Y. Yun, J.H. Choi, Y. Ra, et al., “Monocharged electret-based liquid-solid interacting triboelectric nanogenerator for its boosted electrical output performance”, Nano Energy, **2020**, 70, 104541.

(63) K.M.T. Negara, I.N.G. Wardana, D. Widhiyanuriyawan, N. Hamidi, “Role of the slope on Taro leaf surface to produce electrical energy”, IOP Conf. Series: Materials Science and Engineering, **2019**, 494, 012084.

(64) Y. Liu, Y. Zheng, T. Li, D. Wang, F. Zhou, “Water-solid triboelectrification with self-repairable surfaces for water-flow energy harvesting”, Nano Energy, **2019**, 61, 454-461.

(65) W. Xu, X. Zhou, C. Hao, H. Zheng, Y. Liu, X. Yan, et al., “SLIPS-TENG: robust triboelectric nanogenerator with optical and charge transparency using a slippery interface”, National Science Review, **2019**, 6, 540-550.

(66) J. Chung, H. Cho, H. Yong, D. Heo, Y.S. Rim, S. Lee, “Versatile surface for solid-solid/liquid solid triboelectric nanogenerator based on fluorocarbon liquid infuse surfaces”, Science and Technology of Advanced Materials, **2021**, 21, 139-146.

(67) H. Cho, J. Chung, G. Shin, J.Y. Sim, D.S. Kim, S. Lee, et al., “Toward sustainable output generation of liquid-solid contact triboelectric nanogenerators: The role of hierarchical structures”, Nano Energy, **2019**, 56, 56-64.

(68) J. Chung, D. Heo, B. Kim, S. Lee, “Superhydrophobic water-solid contact triboelectric generator by simple spray-on fabrication method”, Micromachines, **2018**, 9, 593.

(69) J.W. Lee, S.M. Kim, T.Y. Kim, U. Khan, S.W. Kim, “Water droplet-driven triboelectric nanogenerator with superhydrophobic surfaces”, Nano Energy, **2019**, 58, 579-584.

(70) A. Shahzad, K.R. Wijewardhana, J.K. Song, “Contact electrification efficiency dependence on surface energy at the water-solid interface”, Appl. Phys. Lett., **2018**, 113, 023901.

(71) A.N. Parvez, M.H. Rahaman, H.C. Kim, K.K. Ahn, “Optimization of triboelectric energy harvesting from falling water droplet onto wrinkled polydimethylsiloxane-reduced graphene oxide nanocomposite surface”, Composites Part B: Engineering, **2019**, 174, 106923.

(72) J. Niu, W. Xu, K. Tay, G. He, Z. Huang and Q. Wang, “Triboelectric energy harvesting of the superhydrophobic coating from dropping water”, Polymers, **2020**, 12, 1936.

(73) L.E. Helseth, X.D. Guo, “Hydrophobic polymer covered by a grating electrode for converting the mechanical energy of water droplets into electrical energy”, Smart. Mat. Struct., **2016**, 25, 045007.

(74) J. Yu, E. Ma, T. Ma, “Harvesting energy from low-frequency excitations through alternate contacts between water and two dielectric materials”, Sci. Rep., **2017**, 7, 17145.

(75) R.G. Neo, B.C. Khoo, “Towards a larger scale energy harvesting from falling water droplets with an improved electrode configuration”, Applied Energy, **2021**, 285, 116428.

(76) J. Dong, C. Xu, L. Zhu, X. Zhao, H. Zhou, H. Liu, G. Xu, G. Wang, G. Zhou, Q. Zeng and Q. Song, “A high voltage direct current droplet-based electricity generator inspired by thunderbolts”, Nano Energy, **2021**, 90, 106567.

(77) L. Liu, Q. Shi, J.S. Ho, C.K. Lee, “Study of thin film blue energy harvester based on triboelectric nanogenerator and seashore IoT applications”, Nano Energy, **2019**, 66, 104167.

(78) W. Xu, H. Zheng, X. Zhou, C. Zhang, Y. Song, X. Deng, et al., “A droplet-based electricity generator with high instantaneous power density”, Nature, **2020**, 578, 392-396.

(79) H. Wu, N. Mendel, S. van der Ham, L. Shui, G. Zhu and F. Mugele, “Charge trapping-based electricity generator (CTEG): An ultrarobust and high efficiency nanogenerator for energy harvesting from water droplets”, Adv. Mater., **2020**, 32, 2001699.

(80) N. Zhang, H. Gu, K. Lu, S. Ye, W. Xu, H. Zheng, et al., “A universal single electrode droplet-based electricity generator (SE-DEG) for water kinetic energy harvesting”, Nano Energy, **2020**, 82, 105735.

(81) N. Zhang, H. Gu, H. Zheng, S. Ye, L. Kang, C. Huang, et al., "Boosting the output performance of volume effect electricity generator (VEEG) with water column", Nano Energy, **2020**, 73, 104748.

(82) H. Wu, Z. Chen, G. Xu, J. Xu, Z. Wang and Y. Zi, "Fully biodegradable water droplet energy harvester based on leaves of living plants", ACS Appl. Mater. Interfaces, **2020**, 12, 56060-56067.

(83) X. Xu, Y. Wang, P. Li, W. Xu, L. Wei, Z. Wang and Z. Yang, "A leaf-mimic rain energy harvester by liquid-solid contact electrification and piezoelectricity", Nano Energy, **2021**, 90, 106573.

(84) J. Xiong, M.F. Lin, J. Wang, S.L. Gaw, K. Parida, P.S. Lee, "Wearable all-fabric-based triboelectric generator for water energy harvesting", Advanced Energy Materials, **2017**, 7, 1701243.

(85) Y.C. Lai, Y.C. Hsiao, H.M. Wu, Z.L. Wang, "Waterproof fabric-based, multifunctional triboelectric nanogenerator for universally harvesting energy from raindrops, wind, and human motions and as self-powered sensors", Advanced Science, **2019**, 6, 1801883.

(86) E.L. Pradeesh and S. Udhayakumar, Microsystem Technologies, "Investigation on the geometry of beams for piezoelectric energy harvester", **2019**, 25, 3463-3475.

(87) E.L. Pradeesh, S. Udhayakumar, M.G. Vasundhara and K. Nijandhan, "Design and development of frequency tuneable vibration based piezoelectric energy harvester", Ferroelectrics, **2021**, 584, 85-99.

(88) W.C. Elmore and M.A. Heald, "Physics of waves", McGraw-Hill, 1969.

(89) G. Hao, X. Dong, Z. Li and X. Liu, "Water drops impact on a PVDF cantilever: droplet dynamics and voltage output", Journal of Adhesion Science and Technology, **2021**, 35, 485-503.

(90) D. Bartolo, C. Josserand and D. Bonn, “Retraction dynamics of aqueous drops upon impact on non-wetting surfaces”, J. Fluid Mech., **2005**, 545, 329-338.

(91) K. Range and F. Feuillebois, “Influence of surface roughness on liquid drop impact”, J. Coll. Int. Sci., **1998**, 203, 16-30.

(92) A. Imeson, R. Vis and E. de Water, “The measurement of water-drop impact forces with a piezo-electric transducer”, Catena, **1981**, 8, 83-96.

(93) D. Soto, A.B. De Lariviere, X. Boutillon, C. Clanet and D. Quere, “The force of impacting rain”, Soft Matter, **2014**, 10, 4929-4934.

(94) J. Wang, G. Hu, Z. Su, G. Li, W. Zhao, L. Tang and L. Zhao, “A cross-coupled dual-beam for multi-directional energy harvestimg from vortex induced vibrations”, Smart Mater. Struct., **2019**, 28, 12LT02.

(95) G. Hu, J. Liang, C. Lan and L. Tang, “A twist piezoelectric beam for multi-directional energy harvesting”, Smart Mater. Struct., **2020**, 29, 11LT01

(96) J. Wang, S. Gu, A. Abdelkefi, M. Zhang, W. Xu and Y. Lai, “Piezoelectric energy harvesting from flow-induced vibrations of a square at various angles of attack”, Smart Mater. Struct., **2021**, 30, 08LT02.

(97) B. Bao and Q. Wang, “A rain energy harvester using a self-release tank”, Mechanical Systems and Signal Processing, **2021**, 147, 107099.